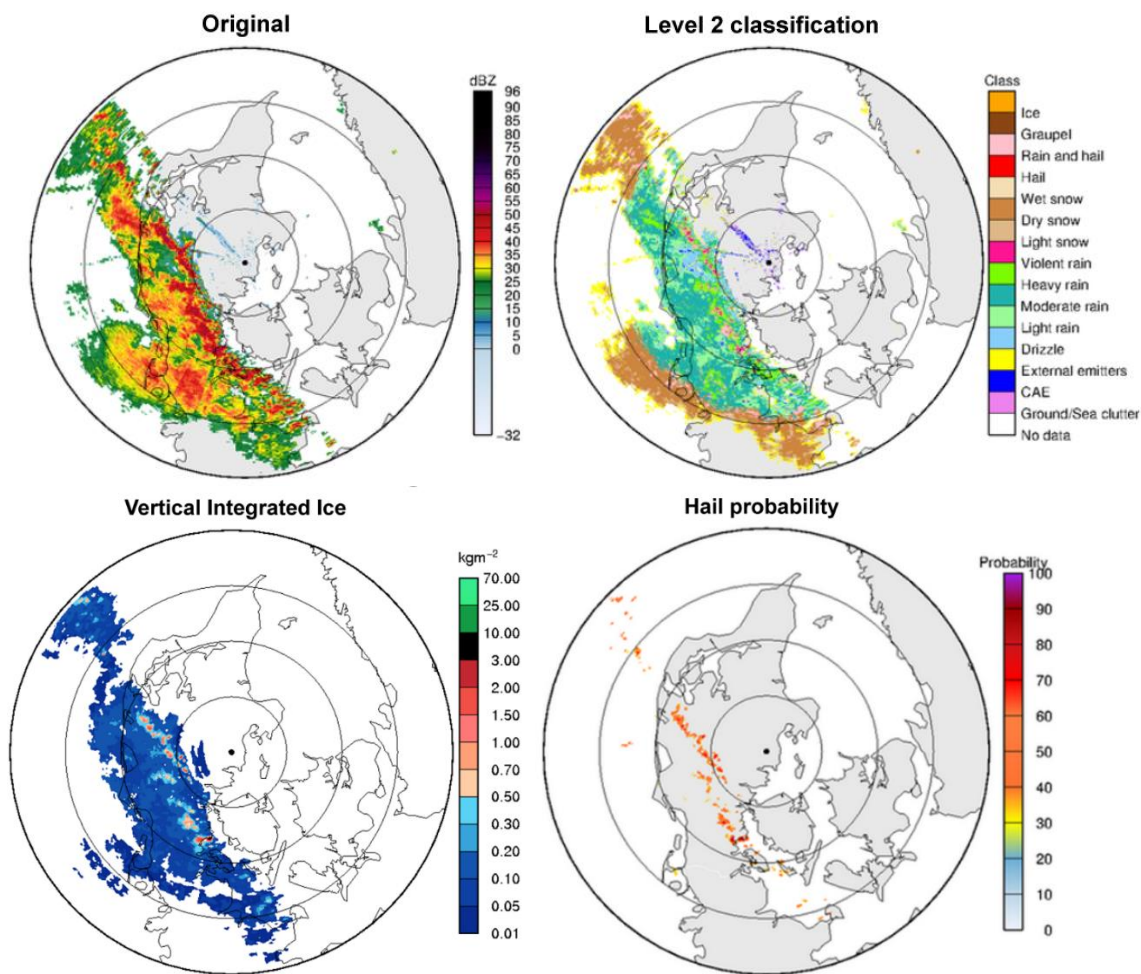


EROSION

D3.3 Present methodology for and evaluation of precipitation erosion warning based on radar data



Deliverable: D3.3 (Public)

Author: Flemming Vejen (DMI)

Publication: December 2021

INNOVATIONSFONDEN / ØSTERGADE 26 A, 4. SAL / 1100 KØBENHAVN K / W: INNOVATIONSFONDEN.DK
www.rain-erosion.dk

D3.3 Erosion warning methodology

Copyright:

Forsidefoto: Radar products 28 July 2018 for Virring. Upper left: radar reflectivity. Upper right: classification of hydrometeors and non-meteorological targets. Lower left: vertical integrated ice (kg/m^2). Lower right: probability of hail.

Udgivet af: Institut for Vindenergi, Frederiksborgvej 399, Bygning 125, 4000 Roskilde

Rekvireres: www.vindenergi.dtu.dk

Preface

This report describes the methodology for, and evaluation of precipitation erosion warning based on radar data for the EROSION project.

The project is funded by Innovation Fund Denmark and project partners. The project period is from April 1st, 2017, to March 31st, 2020 (3 years), and is further extended to December 31st, 2021.

The aim of the project **EROSION – Wind turbine blade erosion: Reducing the largest uncertainties** is to create knowledge and methods to avoid blade erosion caused by rain and hail. The hypothesis is that by reducing the tip speed of the blades, where rain and hail cause severe blade erosion, a significant extension of blade lifetime can be obtained with reduced maintenance cost and negligible loss of production.

The key objective of EROSION is to enable longer lifetime of wind turbine blades at multi-MW machines. To achieve the objective the project work will include testing of specimen in the rain erosion tester and investigation and analysis of damage on leading edges of blades. Furthermore, the rain in real atmosphere will be investigated from ground-based instruments (disdrometers) and modelling of rain based on rain radar data. Finally, a new prototype instrument will be developed to measure rain at wind turbines for making decision on control, to set 'erosion safe mode' with regulation of turbines. Much longer lifetime of wind turbine blades and reduced operation and maintenance costs are expected.

Project website is <http://www.rain-erosion.dk/>

Contents

Preface.....	3
Executive summary.....	5
1 Introduction.....	6
2. Evaluation of radar-based erosion safe mode warning system	8
2.1 Introduction	8
2.2 Radar data and ground observations.....	8
2.3 Using radar products in erosion safe mode operation	9
2.3.1 Radar nowcasting of rain intensity.....	9
2.3.2 Radar classification of hydrometeor type	10
2.3.3 Radar hail probability	11
2.4 Evaluation of nowcasting - examples	11
2.4.1 Principles of verification	11
2.4.2 Fuzzy verification	12
2.4.3 Verification metrics	13
2.4.3 Verification data	14
2.4.4 Examples of evaluation of radar nowcasting of rain	15
2.4.5 Evaluation of conversion between radar reflectivity and rain rate	16
2.5 Evaluation of hail detection products	19
2.4.1 Hail and graupel observations in Voulund	20
2.4.2 Evaluation of radar classification of hail for Voulund area	22
3. Closing remarks	26
References.....	27

Executive summary

One of the project goals is to develop 10-min precipitation erosion warning forecasts based on dual-pol radar data. In this report, the radar-based forecasting is evaluated and assessed. Different radar products are found useful for a blade erosion warning system: radar reflectivity for which the prediction of potentially damaging rain events is based on calculation of the motion field of radar echoes, classification of hydrometeor type using a fuzzy logic method, calculation of vertical integrated ice, and probability of hail.

Rain rates and hail detection are evaluated against disdrometer and rain gauge data to increase knowledge about quality and uncertainty of the radar products. It was expected that it would be possible to monitor and perform nowcasting for a site in Sweden with wind turbines, but the partner RWE could not obtain permission. Instead, the work is done comparing radar data to ground-based data from the HOBE test field at Voulund.

Results from radar-nowcasting have been stored only for a relatively short period for the area around Voulund. Profound analyses of results are not possible, but some examples are selected to illustrate typical challenges in nowcasting. In many cases a quite good match between predicted and observed wet and dry periods, and high and lower absolute values, is seen, but we also see examples of prediction failures in cases where heavy showers are popping up in very short time.

We use a simple mean field bias adjustment of radar data for Voulund area well knowing that this method probably introduces uncertainty and bias. Nevertheless, the simple method shows reasonable results for some show case events. A general Z-R power law is calculated for all rain events in the period 2012-2017 in Voulund, but it has a surprisingly high pre-factor and exponent. The point of using one power law for the whole period is to demonstrate the need for the use of a more advanced QPE method in nowcasting than a standard like Marshall-Palmer, or mean field bias, adjustment.

Detection and prediction of hail by radar have potential for strengthening the decision-making basis for controlling wind turbines in relation to erosion safe mode. Hydrometeor classification and probability of hail products have been evaluated for approx. 135 events for the period 2014-2018 using ground observations of rain amount and hydrometeor type from the HOBE test field in Voulund. Since radar results have only been stored as graphics the evaluation is done by manual inspection of Rømø and Verring radar products.

Disdrometer data from Voulund show that for the period 2012-2018 the annual average duration of hail and graupel is 3:17 hours. It is most frequent in spring and summer but rarely observed in winter. Hail is observed approx. 35 minutes per year. Since hail/graupel of even short duration can cause large damage, the observed frequency indicate that prediction of hail should be given high priority. The manual evaluation shows promising results with a quite good correlation between the radar detected probability and ground observations of hail/graupel, and the radar seems to provide a pretty good indicator for the risk of hail. The level 2 classification was evaluated manually for 108 hail events over the period 2012-2018. The results show that when the radar classification indicates hail/graupel the ground observations generally indicate much higher frequency of these hydrometeors than when the radar doesn't except for slight graupel.

The results demonstrate that combination of various relevant radar products could be very useful in a warning system, which will thus have a great potential to prevent or reduce damage to wind turbine blades caused by heavy rain and ice particles like hail.

1 Introduction

In the EROSION project the research hypothesis is that large raindrops cause significant erosion at the leading edges of wind turbine blades. The research hypothesis is sketched in Figure 1.



Figure 1: Sketch of the research hypothesis in the EROSION project.

One of the project goals is to develop and demonstrate prototype device for precipitation monitoring on wind turbines and to develop 10-min precipitation erosion warning forecasts based on novel rain radars.

Rain forecasting based on dual-polarization radar is developed for hourly wind farm operation planning, as supplementary to in-situ rain observations. By combining data from the DMI’s weather radar network, short term forecasts (nowcasting), is made every 10 minutes. In particular, the aim of the model is to provide information of the likely precipitation intensities, plus information on the precipitation type with a lead time relevant for Erosion Safe Mode (ESM) management at wind farms.

Sagsnr. 6154-00018B

Results from WP1, including statistics and data series on key meteorological parameters, has supported development of the nowcasting model for calculation of potential risk of eroding conditions at wind farm level.

Many studies have shown that droplet size distribution (DSD) and rain intensity is related (e.g., Best, 1950, Kubilai et al., 2013). Key parameters in calculation of droplet kinetic energy and erosion class are drop size distribution (DSD), liquid volume and terminal fall speed (e.g., Assouline, 2009). Furthermore, hydrometeor type, wind speed and blade tip speed must probably be incorporated to achieve realistic estimates of impact kinetic energy and erosion classes at wind farms.

Therefore, one basic idea is to utilize dual-pol radar products, such as rain rates, instead of DSD parameters to process real-time calculation and prediction of droplet kinetic energy and erosion classes. To support and evaluate this idea, disdrometer measurements have been established at selected sites to increase knowledge about the relationship between drop size distribution (DSD), rain intensity and kinetic energy.

The content of this report is a presentation of examples of performance and evaluation of the methodology for erosion warning based on radar data for the EROSION project. The focus is on nowcasting on heavy rain and the potential for prediction of hail and graupel using algorithms developed and implemented at DMI over the years as part of the DMI Radar Operational Products System (DROPS) (Gill, 2010).

2. Evaluation of radar-based erosion safe mode warning system

2.1 Introduction

In this report, nowcasting of precipitation using weather radar observations is evaluated. In Vejen, Bøvith and Gill (2019), different radar products are presented that may be useful in a blade erosion warning system. These includes (1) prediction of potentially damaging heavy rain based on a prototype of the radar data based nowcasting model, (2) classification of hydrometeor type, especially for detection and calculation of probability of hail, (3) calculation of fall velocity and size of hydrometeors.

In Hasager et al (2020), rain gauge and wind speed measurements are used for calculation of erosion and expected lifetime using two different damage increment models. The point is that rain rate observations can be used in a damage control model, thus it is obvious that nowcasting of rain intensity using radar data is the key stone in first version of a safe mode decision system. Detection of probability of hail could supplement such a system with valuable information.

At DMI many efforts have been put to development of a nowcasting model which is based on advection of radar observations using a motion vector field from the movement of the precipitation patterns in time sequences of radar images. Opposite to this, computation of fall velocity and hydrometeor size products at DMI is still in a very early stage. More work on routinely calibration to ensure good quality of the dual polarization parameter, differential reflectivity, is required to account for potential biases. Therefore, it is too early to introduce these two products in calculation of kinetic energy and potential erosion level for use in a prototype erosion safe mode model.

The present report focuses on evaluation of the capability of DMI's nowcasting model to predict heavy rain events, and on evaluation of the hail product. Hail probability and rain rates calculated from dual-polarization radar will be evaluated against disdrometer and rain gauge data to increase knowledge about quality and uncertainty of the radar products.

2.2 Radar data and ground observations

DMI operates a radar network of five dual-polarization (dual-pol) C-band Doppler weather radars (Figure 2), hereafter called dual-pol. A dual-pol weather radar is a remote sensing instrument that measures reflectivity of objects in two polarizations, horizontal and vertical, in a volume in the atmosphere. The radar scans in azimuth at several elevations and detects the atmospheric content of hydrometeors and their properties. The radar network provides radar data in high temporal and spatial resolution, i.e., 500×500 m² pixel size and 10-minute scans up to 240 km range.

Various sophisticated parameters (or moments) are measured by dual-pol radar technology. Dual-pol moments can be used in hydrometeor classification algorithms (e.g., Straka, Zrníc and Ryzhkov, 2000), and the classification method used at DMI is described in Gill, Sørensen and Bøvith (2012) and ERAD conference proceedings (Gill, Overgaard and Bøvith, 2008, Gill et al, 2010, Gill et al, 2012b). Radar measurements of reflectivity caused by meteorological targets are used as input to the nowcasting model.

Sagsnr. 6154-00018B

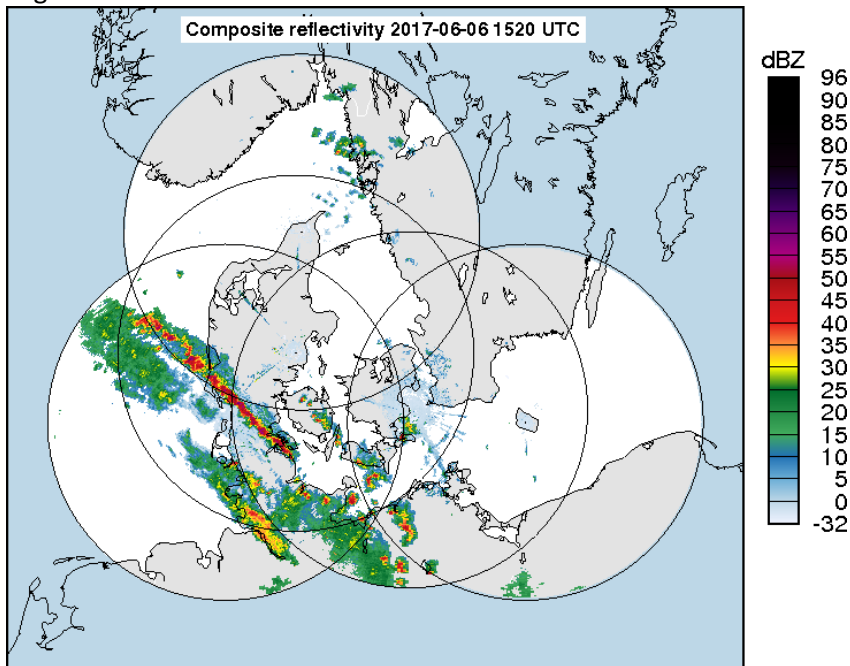


Figure 2: DMI's weather radar network shown with an example from 6 June 2017 at 1520 utc. The unit dBZ indicates the relative rain rate.

Several disdrometers are installed during EROSION WP1 (Hasager and Vejen, 2017), while disdrometer and rain gauge data are provided from a test field in Voulund¹ operated by the HOBE project² in the period 2009-2019. A description of Voulund testfield can be found in Vejen et al (2018).

2.3 Using radar products in erosion safe mode operation

2.3.1 Radar nowcasting of rain intensity

Precipitation often displays a very high temporal and spatial variability and is therefore difficult to predict accurately at small scales and a long time in advance. The highest accuracy of precipitation forecasts at fine scale is currently regarded to be obtained from radar-based nowcasting models, but these models are only superior to more advanced meteorological models at the very short lead times (less than 2-3 hours).

The DMI radar nowcasting model is a simple advection model based on 1) the computation of a motion vector field from a time sequence of radar images using an optical flow algorithm and 2) the advection of the most recent radar image along the motion vector field. In the DMI implementation the Farneback algorithm is used (open-source library, Bradski and Kaehler, 2008) which assumes and produces a spatially smooth motion vector field. A temporally smooth evolution of the motion field is obtained by exponential smoothing of the motion field as proposed in Bowler, Pierce, and Seed (2006). The advection step is performed using a semi-Lagrangian backward interpolation scheme carried out using one-step cubic interpolation from a given lead time and back to the observation time. More information about the DMI nowcasting is found in Vejen, Bøvith and Gill (2019).

¹ The Voulund site is a hydrological test field. The site was serviced and operated in co-operation between Aarhus University, DTU, University of Copenhagen, GEUS and DMI.

² Center for Hydrology - a Hydrological Observatory and Exploratorium.

Sagsnr. 6154-00018B

The radar nowcast method has the potential to provide accurate and timely input for the “erosion safe-mode” algorithm for wind turbine control.

Radar data can be affected by various sources of error and may introduce biases in nowcasting of rain. For example, severe false echoes from ground targets may be seen during temperature and humidity inversions causing downward bending of the radar beam. Range dependent biases are related to the vertical variation in the reflectivity profile with distance, and at larger ranges the radar beam is far above the ground and may overshoot more shallow precipitation. More background information about errors in radar detection of hydrometeors can be found in Šálek et al. (2004). Fortunately, severe false echoes are not common during precipitation. However, DMI’s radar products are of very high quality that contain very few false echoes as has been demonstrated over the years in an operational environment.

Radar measurements of backscattering from hydrometeors provides a snapshot of the state of the atmosphere in terms of precipitation, and the so-called radar reflectivity, Z , is related to the drop size distribution (DSD) through $Z = \sum nD^6$, where n =number of droplets and D =droplet diameter (Battan, 1973). Extensive research has revealed that Z is related to the rain rate, R , through a general empirical expression of the form $Z = AR^b$, where A and b are constants (Battan, 1973), which allow us to calculate the “true” nowcasted rain rate. A widely used Z - R relation is that for stratiform rain developed by Marshall and Palmer (1948), but biases are introduced using this relation if the precipitation is not stratiform. Many Z - R relations have been developed for a large range of precipitation types (e.g., Šálek et al., 2004), thus a better approach could be to use a more appropriate equation. On the other hand, because of the large variability of DSD in time and space, significant uncertainty is introduced into the conversion of Z to R . A more reliable and commonly used approach is to adjust radar estimates of rain rate against ground measurements of rain such as rain gauges.

At DMI, SQPE estimation technique (Surface Quantitative Precipitation Estimate) based on Kriging methods has been developed (private communication, Gill, 2019). However, more work is required before application of reliable rain gauge adjustment in nowcasting. The processing time of rain gauge adjustment is challenged by the fast evolution often seen in convective rain, and a certain number of rain gauges are required to keep the uncertainty of the adjustment as low as possible.

2.3.2 Radar classification of hydrometeor type

A hydrometeor classifier (HMC) using a fuzzy logic method has been developed and implemented at DMI inspired by methods reported in the open literature (Gill, Sørensen and Bøvith, 2012a, and ERAD conference proceedings (Gill, Overgaard and Bøvith, 2008, Gill et al, 2010, Gill et al, 2012b)). The classifier makes use of the dual-pol parameters³ Z_{HH} , Z_{DR} , K_{DP} , ρ_{HV} , plus the texture parameters associated with Z_{HH} , Z_{DR} , K_{DP} . In the current version of the algorithm, a radar echo can be classified into 12 classes: (1) ground clutter, (2) sea clutter, (3) electrical signals from external emitters that interfere with our radars, (4) clean air echoes (CAE) such as from birds and insects, (5) drizzle, (6) light rain, (7) moderate rain, (8) heavy rain, (9) violent rain, (10) light snow, (11) moderate to heavy snow, (12) rain/hail mixture. The DMI’s hydrometeor classifier has been manually evaluated over the last many years and has been found to give reliable results. However, validating the HMC is very challenging as the product shows the hydrometeor class in the atmosphere which is not necessarily what is observed on the Earth’s surface.

The current version of the algorithm firstly does a so-called level 1 classification where a radar echo is classified into one of four simple classes (precipitation, clutter, clean air echoes, and external emitters), and secondly, a level 2 classification, where the echoes classified as precipitation in level 1 are further sub-classified into the 12 precipitation classes mentioned above. In this case the heights of the melting layer

³ Z_{HH} = corrected reflectivity, Z_{DR} = differential reflectivity, K_{DP} = specific differential phase, ρ_{HV} = cross-correlation coefficient between the horizontal and vertical polarized waves, Φ_{DP} = differential phase shift.

Sagsnr. 6154-00018B

computed by the local NWP model are used to strengthen the classification between the different classes of rain and snow. Figure 3 shows an example of the level 2 classification. The algorithm can make use of the classification output to remove the non-meteorological echoes in the original radar reflectivity product, Z_{HH} .

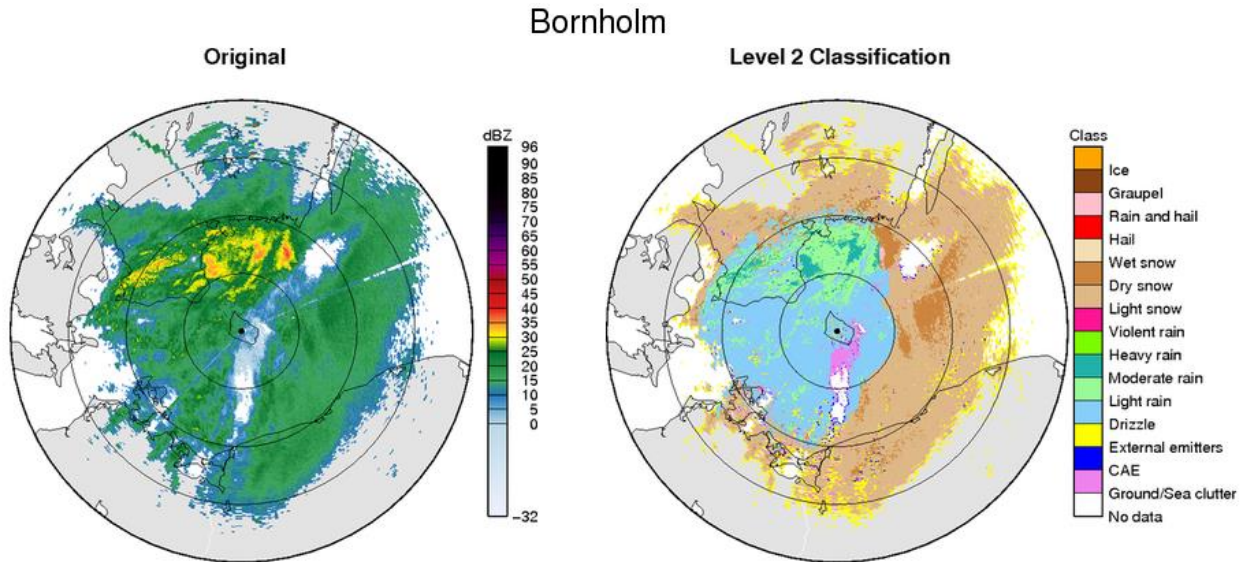


Figure 3: Shows radar image on the left (original) and its corresponding level 2 hydrometeor classifications into eleven classes.

2.3.3 Radar hail probability

A radar based probability of hail (POH) product has been developed at DMI also inspired by methods reported in the open literature (private communication, Gill, 2008, Delobbe and Holleman, 2003). The product has been manually validated over the last many years against reported hail events and has been found to be reliable.

In Figure 4 is seen an example of DMI's POH-product. Several heavy showers are located over Zealand, and especially one with very high rain rate ($\text{dBZ} > 40$) near Køge is associated with a hail probability of 70-75 percent. Severe hail was reported from ground observations.

2.4 Evaluation of nowcasting - examples

2.4.1 Principles of verification

In classical validation, it is examined how well a given nowcasting model within certain limits can predict a value point by point when compared with independent data. However, such an approach is not fair in relation to nowcasting of precipitation, as there can be great spatial and temporal variability in rainfall intensity, especially in showers due to complex convective processes. A forecast may be a success even though spatial and temporal changes of the values are observed in the areas being compared.

An example is shown in Figure 5. If a nowcasting is verified pixel by pixel, the quit high rain rate observed in the small black square is seen to be poorly predicted, even with a 10-minute lead time. But it is also seen that the observed heavy rain is only marginally shifted to the east and that high and low values in other pixels are quite well predicted. The pattern of the rain has changed, but the location of heavy rain is oriented almost as predicted in a NW-SE band with slight rain to the SW and NE.

Sagsnr. 6154-00018B

Stevns 2018-09-24 1400 UTC

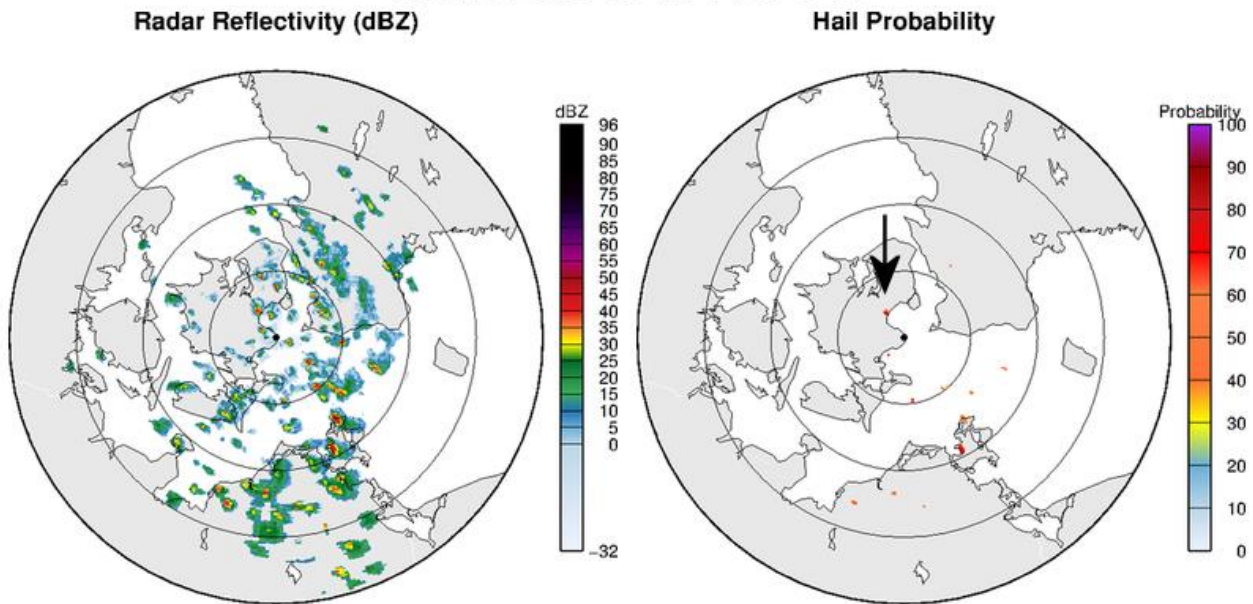


Figure 4: Radar products showing radar reflectivity and hail probability. The arrow is pointing at a heavy shower with high probability of hail. Damage caused by hail was reported in an industrial area in Køge (arrow).

The example illustrates that it is fairer to the nowcasting to verify on matrix level due to the spatial and temporal variability of rain.

2.4.2 Fuzzy verification

Fuzzy verification compares matrices of any given dimension to control for comparability between predicted and observed rain area, e.g., if a predicted rain rate above a threshold, $W \geq R_{thrs}$, is detected within an appropriately small area of observed pixels, $s \times s$. Thus, if the nowcasting predicts a cloud burst within say $5 \times 5 \text{ km}^2$ (10×10 radar pixels) and this is later observed within the area, i.e., $W \geq R_{thrs}$ and $R \geq R_{thrs}$, it is regarded as a successful prediction regardless of the pixel-by-pixel match of the rain rate level.

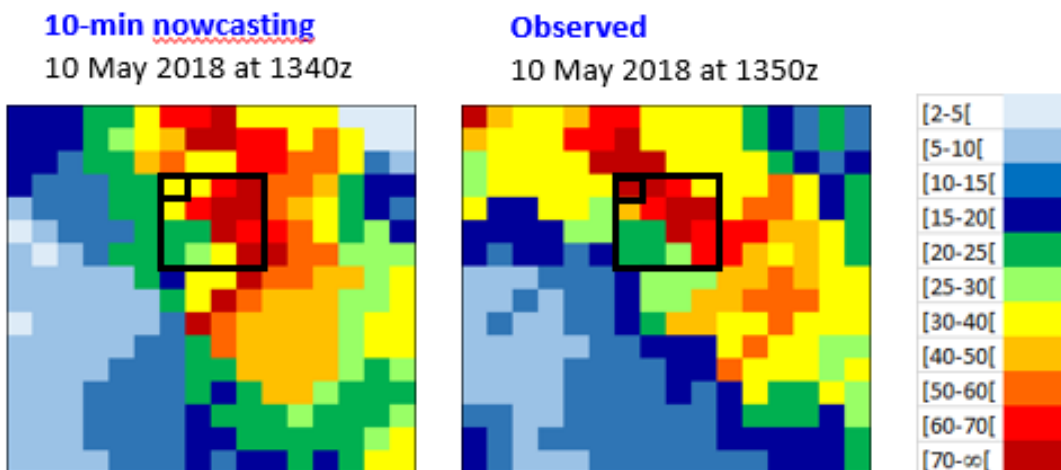


Figure 5: Changes in reflectivity level (mm/hour) during a 10-minute period 10 May 2018 for DMI's radar on Rømø. Pixel size is $500 \times 500 \text{ m}^2$.

Sagsnr. 6154-00018B

It should be possible to get an idea of the forecast quality as function of scale by experiments with the dimension, $s = \{1, 2, \dots, S\}$, where S is chosen large enough to contain typical convective small-scale systems like individual showers. It has not been possible within the scope of the project to conduct such experiments, thus $s = 8$ corresponding to 8×8 pixels or $4 \times 4 \text{ km}^2$ are chosen for general use, which we think is appropriate for verification of the nowcasting.

We use a fuzzy verification technique proposed by Ebert (2008). For each observed rain rate, R_i , within the matrix we use the parameter, $\langle I \rangle_s$, as an indicator of exceedance of a threshold value, R_{thrs} . In our decision model, $\langle I \rangle_s$ is considered a discrete variable, i.e., it is assigned a value of 0 ($R_i < R_{thrs}$) or 1 ($R_i \geq R_{thrs}$), which is in accordance with the “yes/no” principle behind ESM.

In the following an event is defined as a case where observed or predicted rain rate exceeds a threshold, i.e., that $R_{nwc} \geq R_{thrs}$ or $R_{obs} \geq R_{thrs}$. If the probability of an event is calculated as the fraction of events in an area of dimension s , probabilistic verification can be established by:

$$\langle P_{obs} \rangle_s = \frac{1}{N} \sum_{i=1}^N \langle I_{obs(i)} \rangle_s \text{ where } I_{obs(i)} = \begin{cases} 0 & \text{if } R_i < R_{thrs} \\ 1 & \text{if } R_i \geq R_{thrs} \end{cases}$$

$$\langle P_{nwc} \rangle_s = \frac{1}{N} \sum_{i=1}^N \langle I_{nwc(i)} \rangle_s \text{ where } I_{nwc(i)} = \begin{cases} 0 & \text{if } W_i < R_{thrs} \\ 1 & \text{if } W_i \geq R_{thrs} \end{cases}$$

Here, $\langle P_{obs} \rangle_s$ = fraction of pixels in a matrix with observed events, and $\langle P_{nwc} \rangle_s$ = fraction of pixels in a matrix with predicted events, where N = number of pixels in the matrix. Instead of comparing predicted and observed events pixel by pixel, the above makes it possible to calculate an error that is independent of scale and is based on a comparison of pixel values $\langle R \rangle_s$ and $\langle W \rangle_s$ within the window. The procedure for fuzzy verification is quite simple:

- Select a scale $s = \{1, 2, \dots, S\}$, in our experiment $s = 8$.
- Select rain rate thresholds with index values $k = \{1, 2, \dots, K\}$ and $R_{thrs} = \{10, 20\}$ [mm/t], corresponding to threshold in Hasager et al (2020) for which fuzzy verification is calculated.
- Extract observation and prediction data.
- For rain rate thresholds, calculate scale dependent values: $\langle I_{obs} \rangle_s$, $\langle I_{nwc} \rangle_s$, $\langle P_{obs} \rangle_s$ and $\langle P_{nwc} \rangle_s$.
- The verification score for the whole radar domain is calculated by moving the matrix window one pixel at a time. The domain size for area around Voulund is 19×20 pixels.
- Calculate verification metrics.

The potential of this technique is that we get a $K \times K$ matrix with a score for each fuzzy verification and with a score varying with rain rate and scale. This makes it possible to identify those combinations of scale and rain rate where a high-resolution forecast is useful. The verification technique can be aggregated over, e.g., months, seasons, and years, to identify and analyze systematic variations in performance. We find such analyzes could be a goal for further research, which has not been possible within the current project.

2.4.3 Verification metrics

A forecast is useful if the frequency of predicted events equals the frequency of observed. The fractions skill score, FSS , is a measure of the success of a nowcasting since it compares the fraction of observed events with the corresponding predicted within a matrix. FSS is calculated by:

Sagsnr. 6154-00018B

$$FSS = 1 - \frac{FBS}{\frac{1}{N}[\sum_N \langle P_{nwc} \rangle_s^2 + \sum_N \langle P_{obs} \rangle_s^2]}$$

Here, *FBS* is the Fractions Brier Score which in the principle is a mean square error:

$$FBS = \frac{1}{N} \sum_N (\langle P_{nwc} \rangle_s - \langle P_{obs} \rangle_s)^2$$

If the forecast is perfect, we get $FSS = 1$, while $FSS = 0$ indicates complete mismatch between observation and nowcast. In addition to *FSS* there are other standard methods for continuous, categorical, and probabilistic verification, e.g., probability of detection, *POD*, false alarm rate, *FAR*, and true skill score, *TSS*. These metrics are calculated using yes/no combinations (value 0 or 1) of the following:

- H = hits (observation correctly predicted)
- F = false alarms (forecast predicts an event that is not observed)
- M = misses (an observed event was not predicted)
- C = correct rejections (forecast correctly predicts that no event was observed)

The fraction of correctly predicted events is given by:

$$POD = \frac{\sum_N H}{\sum_N H + \sum_N M}$$

The fraction of observed non-events wrongly predicted as events is given by:

$$FAR = \frac{\sum_N F}{\sum_N C + \sum_N F}$$

Now, a true skill score is simply calculated as the difference between *POD* and *FAR* to indicate the forecast ability to differentiate between observed hits and observed false alarms, i.e., $TSS = POD - FAR$. Although there are many other verification metrics, we find it efficient to use the above.

2.4.3 Verification data

It was expected to monitor and nowcast for a site in Sweden with wind turbines, but partner RWE could not obtain permission. Instead, the work is done comparing radar data to ground-based data from the HOBE test field at Voulund. Instruments installed and data collected from the Voulund test field are described in Vejen et al (2018).

Results from radar-nowcasting have been stored only for a relatively short period for the area around Voulund and based on these data verification of nowcasting of selected events has been initiated. Due to limitations in selected data profound analyses of results are not possible, but we will show selected examples to illustrate typical challenges in nowcasting. Matrices of $N \times N$ pixels are extracted from radar- and nowcasting data with a lead time of 0-2 hours for selected rain events in 2017.

Sagsnr. 6154-00018B

Rain events of different types have been selected to test the nowcasting model at different weather conditions: (1) heavy isolated showers, (2) more widespread heavy rain, (3) heavy rain popping up in the radar horizon, (4) fast evolving heavy rain with very short warning time.

2.4.4 Examples of evaluation of radar nowcasting of rain

Since the uncertainties of the radar nowcast increase quite quickly with lead time and the uncertainty depends highly on the type of precipitation, we expect higher predictability for wide-spread rain than for scattered, convective rain. Since the heaviest rain is associated with convective systems, we focus on predictability and challenges on such events in the following examples.

It is our experience that it is often easy to track showers long before arrival and that a 10-minute lead time will result in a reasonable nowcasting. The real challenge may be associated with fast evolving convective system causing cloud bursts and hail where nowcasting may fail, even if the lead time is short.

Heavy rain may pop up apparently out of nothing in a sequence of radar images and may cause heavy rain within a time scale of less than 10 minutes as seen in the example in Figure 6 for 19 August 2017. At 9:50z there is nothing to worry about, but during less than 10 minutes a substantial increase of the reflectivity is observed (see arrow pointing at the specific rain cell). Other cells along a SW-NE oriented band of showers are seen to have the same life history which is characterized by a steep development curve. At the same time other cells are starting to decay.

Since the nowcasting is based on advection of the most recent radar image along the motion vector field and does not consider temporal changes in reflectivity, the methodology is challenged in case of fast evolvment as well as decay of rain echoes.

Figure 7 shows predicted and observed radar rain rate for Voulund for two heavy showers in Figure 6, and other smaller showers, passing during 19 August 2017. Note, that the rain rate is adjusted by rain gauges. It is seen, that except for the shower pointed in Figure 6 the rain rate is predicted quite well.

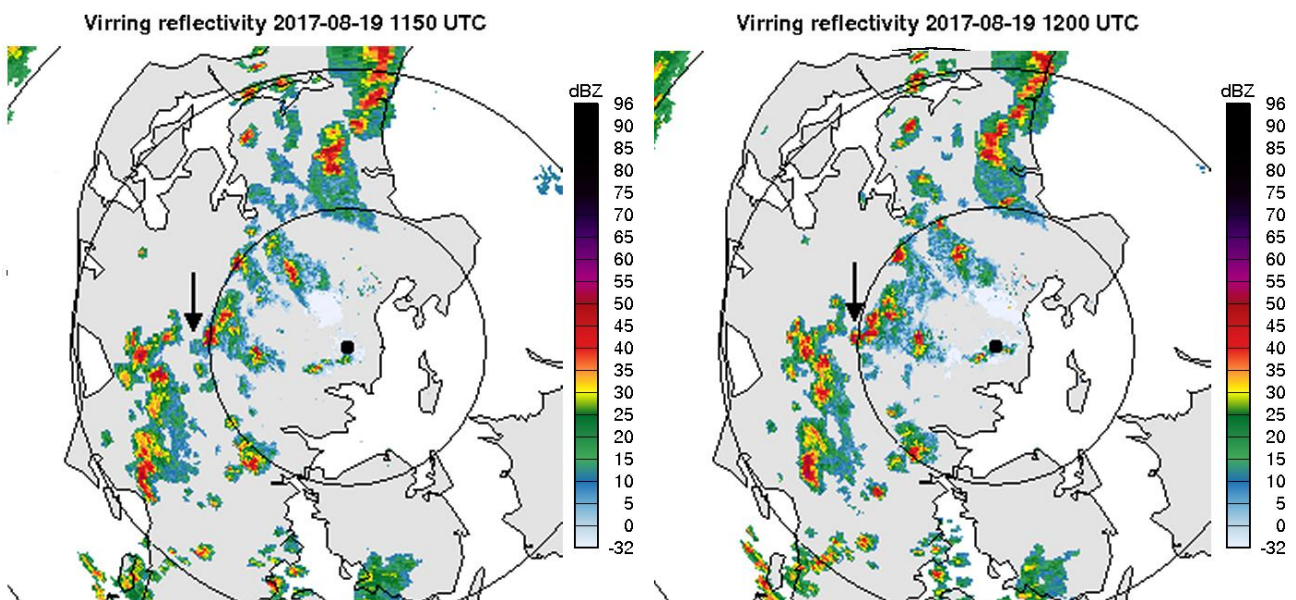


Figure 6. Example of complex shower system along a line, 19. August 2017 at 1150z and 1200z. The arrow points at a fast-developing shower. The reflectivity (dBZ) is from DMI's weather radar on Rømø.

Sagsnr. 6154-00018B

Table 1 shows evaluation statistics for the specific case shown in Figure 6. We use a threshold value of $R_{thrs} = 10$ mm/h to get an idea of the ability of the nowcasting to predict 10 mm/h or more within 10 minutes lead time. At 12:00z the maximum observed pixel value within 8×8 pixels (4×4 km²) were 16,7 mm/h compared to a quite larger predicted maximum value of 24,5 mm/h. For the matrix area the FSS and POD score is high and FAR is low indicating a rather successful nowcasting of the shower passing Voulund (the shower just east of the arrow in Figure 6). The shower that suddenly popped up and passed Voulund 20 minutes later is of reasonable reasons not predicted at all. With a maximum predicted rain rate of 1,2 mm/h, the observed rainfall of up to 20,2 mm/h 10 minutes later was totally missed which explains why the value of FAR = 0. FSS = 0,006 and POD = 0 indicates the low score of the prediction.

Difficulties in prediction of rain rates in the early stage of a heavy shower are only critical if the shower is close to the wind farm. Once the shower is in a stage in its history where it is easy to track the nowcasting becomes more confident, and it will be able to issue more reasonable cloud burst warnings for ESM operation.

Table 1. Verification of nowcasting with lead time 10 for 19 August 2017 at 1200z, 1210z and 1220z using data from DMI's radar on Rømø. Parameters: maxO, maxN = maximum rain rate within a matrix of pixels around Voulund for observed and nowcasted rain rate, respectively. FSS = Fractions Skill Score, POD = probability of detection, and FAR = false alarm rate.

Date	Time	maxO	maxN	FSS	POD	FAR
20170819	1200z	16,7	24,5	0,776	0,897	0,092
20170819	1210z	3,6	12,9	0,208	0,000	0,090
20170819	1220z	20,3	1,2	0,006	0,000	0,000

In Figure 8 we use the same evaluation technique as above for nowcasting for the period 7-9 June 2017, which is a period characterized by moderate, or heavy, showers passing Voulund area. Radar data are adjusted by rain gauge observations. A rain rate of 38 mm/h was predicted for a 10-minute lead time for the heavy shower in the end of the period which compares well with the observed 36 mm/h. Most of the moderate showers are predicted with acceptable success. To get an idea of the representativeness of radar data to local rain in Voulund radar pixels for Voulund are compared with 10-minute rain amount measured with a reference gauge for liquid precipitation installed in Voulund test field. We see a quite good match between wet and dry periods, and high and lower values, detected using radar and rain gauge (Figure 9).

The differences between radar and rain gauge are not surprising since we compare point and area measures where the rain gauge accumulates over 10 minutes while the radar provides a snapshot of the rain rate. For simplicity the radar rain amount is calculated assuming a constant rain rate over the 10-minute period, which introduces additional uncertainty in the comparison if the rain rate is not constant over time.

2.4.5 Evaluation of conversion between radar reflectivity and rain rate

The rain rate, R , and the reflectivity factor, Z , is related through a power law of the form $Z=AR^b$, called a Z-R relation, where A and b are empirical constants (Battan, 1973). The relation between R and Z depends on the hydrometeor type and drop size distribution, and the empirical constants, A and b , shows large variability (Uijlenhoet, 2001) (Figure 10). For example, if a standard Z-R relation like the so-called Marshall-Palmer relation (Marshall and Palmer, 1948) is used ($A=220$, $b=1.60$) for computation of QPE (Quantitative Precipitation Estimate), a bias of unknown magnitude is introduced in the estimates.

Sagsnr. 6154-00018B

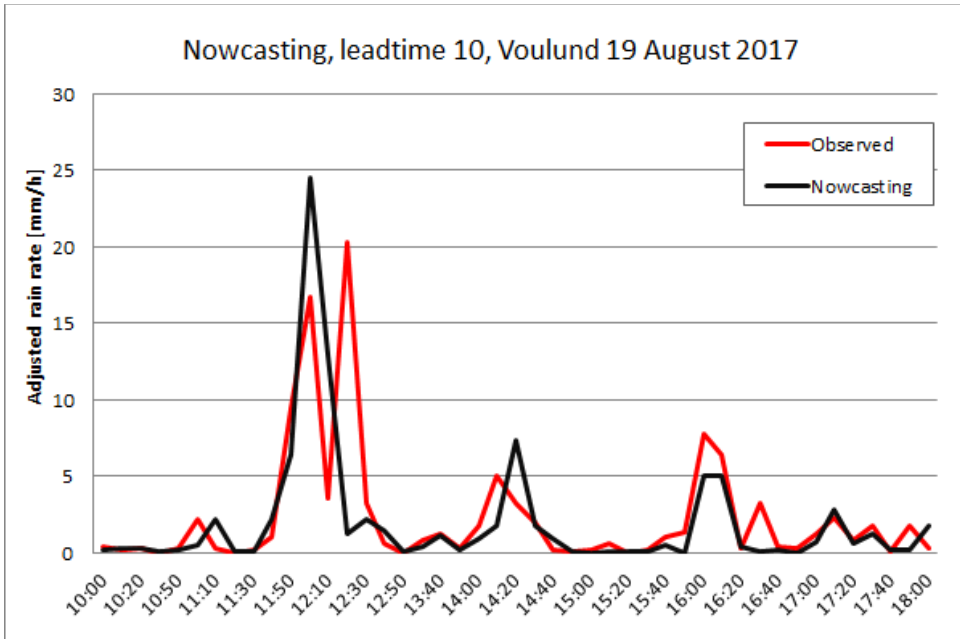


Figure 7. Verification of nowcasting for showers passing Voulund 19 August 2017 using radar data from DMI's weather radar on Rømø. Radar rain rate estimates are adjusted by rain gauge.

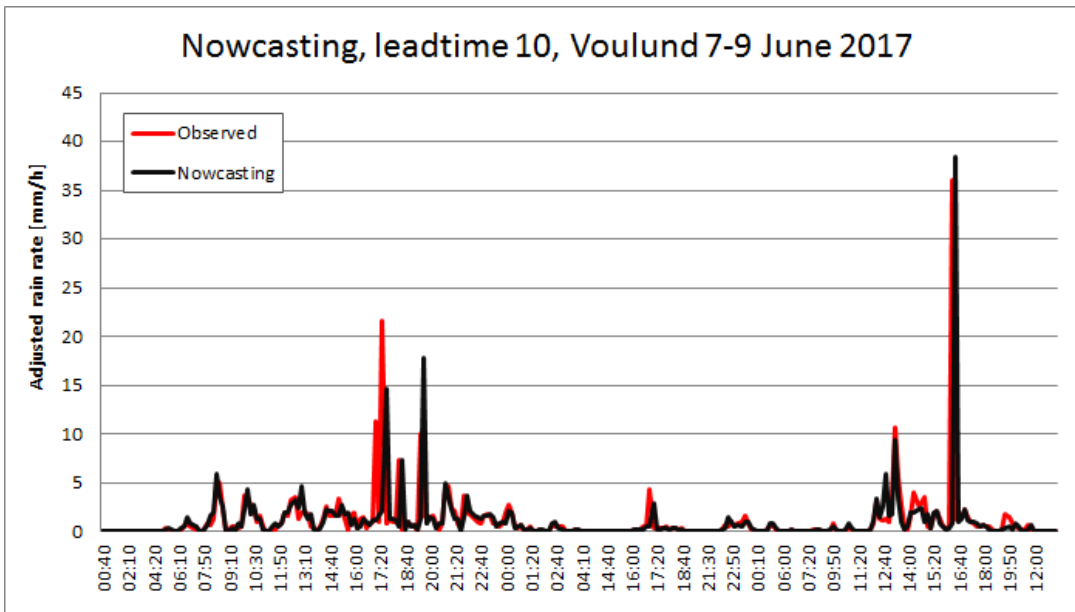


Figure 8. Observed and predicted maximum rain rate within 8×8 pixel matrix for Voulund area for the period 7 June 2017 at 00z until 9 June 2017 at 12z.

To get reliable QPE estimates an alternative to the standard adjustment is required, and several methods for this have been proposed (e.g., Brandes, 1975, Rosenfeld et al, 1994, Michelson et al, 2000, Gabella and Amitai, 2000, Sinclair and Pegram, 2005, Chumchean et al, 2006, Haberlandt, 2007). For the examples for the Voulund area shown in previous section we use a simple mean field bias approach (e.g., Goudenhoofd and Delobbe, 2009) based on 24-hour radar and rain gauge observations where daily adjustment factors are used to adjust 10-minute radar rain rates calculated using the Marshall-Palmer conversion.

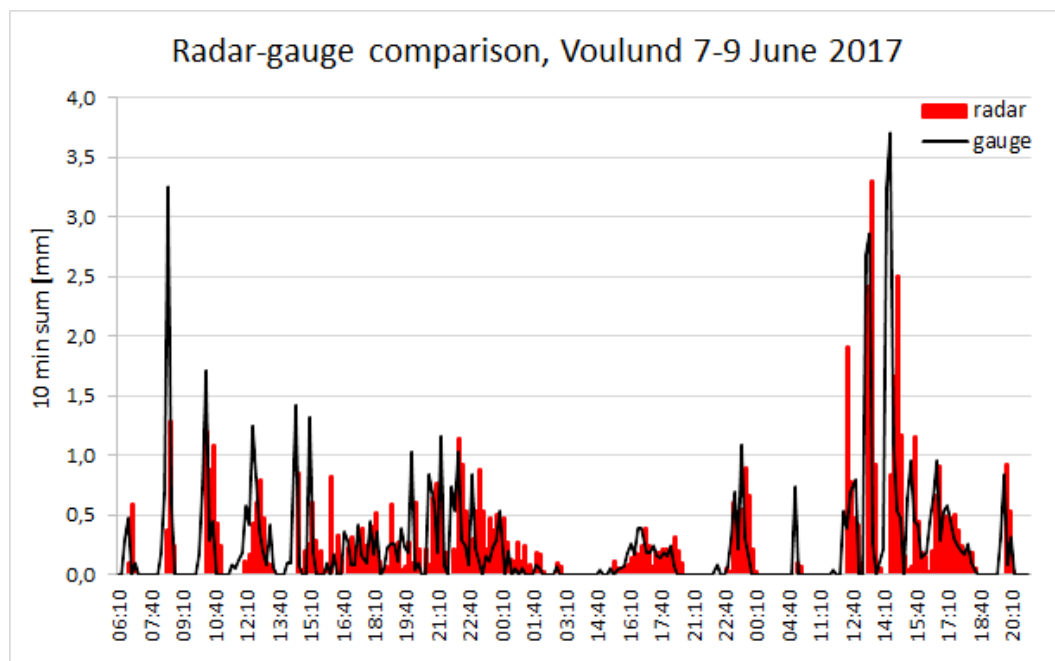


Figure 9. Comparison between precipitation sum measured by a rain gauge in Voulund and radar precipitation adjusted by rain gauge data.

This method may probably introduce increased uncertainty and bias on time scales shorter than 24 hours in cases with variations in precipitation type, because then the factor conversion may not be the right one to apply in all time steps. Nevertheless, this method shows reasonable results for the events shown in Figure 7- Figure 9.

To illustrate the importance of adjusting individual rain event by rain gauges we have calculated a general Z-R power law that for all rain events 2012-2017 in Voulund causes an unbiased cumulative precipitation amount and a 1:1 fit of radar-gauge amounts for individual days (Figure 11). The power law is $Z = 3500R^{1.80}$ with a very high pre-factor, A , and an exponent, b , in the high end.

Not surprisingly, using one power law for the whole period causes a large scatter between measured and calculated daily rainfall. The result seen in Figure 12 is that for this power law any Z-value the corresponding rain rate, R , is much lower than those calculated by power laws for the most common precipitation types at high latitudes (Karlsson, 1997). This is in line with a previous internal investigation at DMI that showed a general underestimation by approximately a factor 2 using Marshall-Palmer.

The point is that we demonstrate a need for the use of a more advanced QPE method in nowcasting than a standard, or mean field bias, adjustment. An advanced QPE method using a Kriging approach for radar-gauge merging is under development at DMI, but it was not possible to make use of this method within the scope of the project.

Sagsnr. 6154-00018B

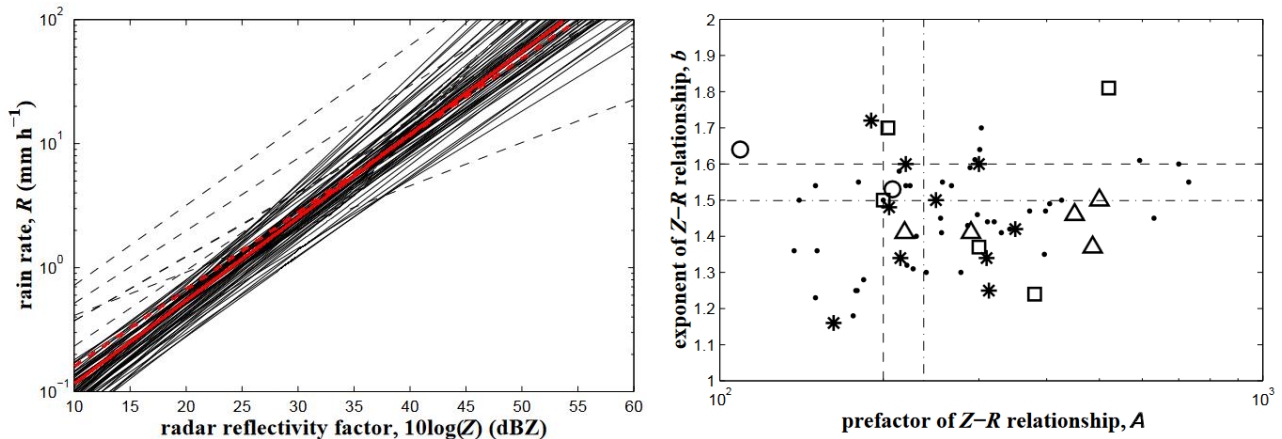


Figure 10. Left: plot of 69 power laws from Battan (1973) including 5 deviating relations (dotted black lines) of which 4 have $A < 100$ and one has $b = 2.87$. Thick red line: average of Battans relations, $Z = 238R^{1.50}$. Dotted red line: $Z = 200R^{1.60}$ from Marshall et al (1955). Right: A and b for the 69 Z-R relations sorted by precipitation type. Circles: orographic. Triangles: thunderstorms. Stars: widespread/stratiform rain. Squares: showers. Dots: identification not possible (Uiljenhoet, 2001).

2.5 Evaluation of hail detection products

The section will have focus on the rain/hail events that may cause significant erosion on turbines. As previously described, DMI has implemented methods for detecting hail using classification of precipitation types and calculating the amount of ice in the atmosphere and probability of hail. It is assumed that these products can support radar nowcasting of heavy rainfall with useful information about the local weather conditions. This enables the decision-making basis for controlling wind turbines in relation to erosion safe mode to be strengthened.

In the following, these methods are evaluated using ground observations of rain amount and hydrometeor type from the HOBE test field in Voulund to increase knowledge about quality and uncertainty of the radar products.

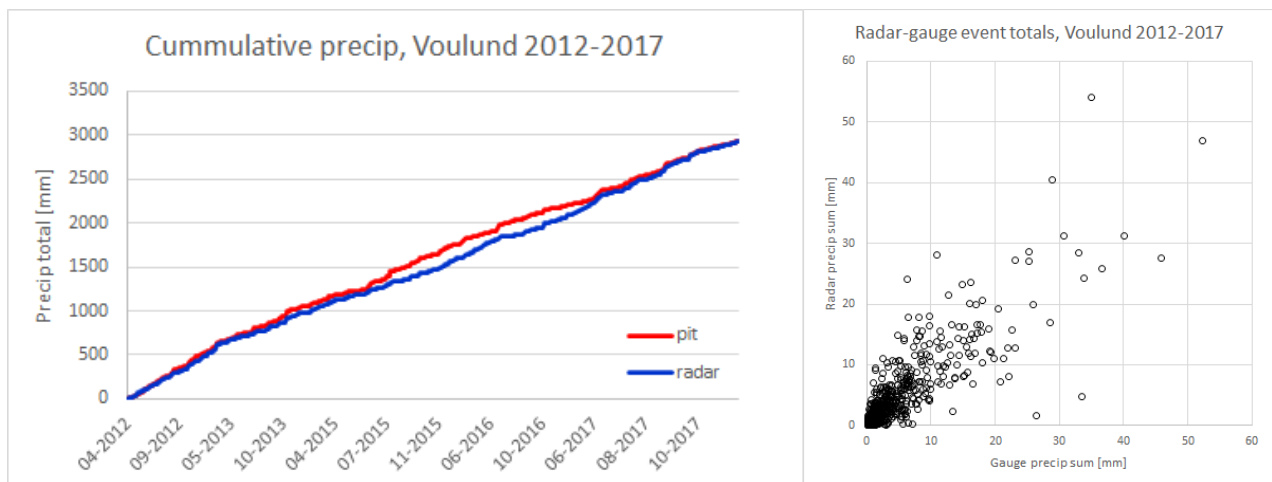


Figure 11. Left: cumulative precipitation over the period 2012-2017 using a standard Z-R relation based on all gauge and radar data for the Voulund test site. Right: the daily sums for the period rain gauges (pit = reference gauge for rain) and standard adjusted radar data.

Sagsnr. 6154-00018B

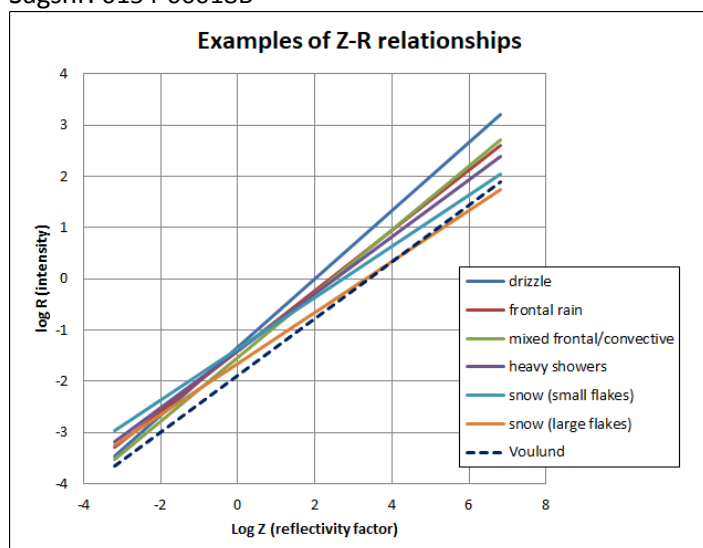


Figure 12. Comparison between Z-R power laws for precipitation types most common at high latitudes (full lines) (Karlsson, 1997) and the Z-R relation calculated for rain events in Voulund for the period 2012-2017 (dotted line).

2.4.1 Hail and graupel observations in Voulund

A disdrometer of type Thies LPM (Laser Precipitation Monitor, LPM) is installed at Voulund and provides the project with hydrometeor type data for the period 2012-2018. The precipitation type is determined using measurements of particle diameter and fall speed. These proportions have been subject to profound research, and for liquid precipitation the relation between terminal fall speed of water droplets in stagnant air (Gunn and Kinzer, 1949) is often referred to as the Gunn-Kinzer line. Figure 13 illustrates the general principles behind classification of different hydrometeors (Löffler-Mang and Joss, 2000), e.g., hail is characterized by high fall speed and large particle sizes.

Field evaluation of LPM has showed promising results in detection of hydrometeor types compared to a present weather sensor of type Vaisala FD12P and other disdrometers like OTT Parcival. According to Haijn and Wauben (2010) LPM is the most promising sensor giving added value to detection of precipitation phase shift from liquid to solid, fog and very light precipitation. However, in their study there were too few data to conclude on LPM's capability to detect hail which is known to be a problematic hydrometeor type for all sensors, but they stated that LPM seems to be better than other sensors. Further field evaluation of LPM reported in Wauben et al (2016) included more hail events, but there was no evidence to reject Haijn and Wauben's statement about LPM hail detection.

LPM is more sensitive and detects more small particles compared to the other instruments, and there are more detections of false precipitation due to dust, spider web and insects (Haijn and Wauben, 2010). Despite the reported uncertainties in hydrometeor type detection, we assume that LPM is a reliable instrument for detection of hail and graupel. Moreover, to avoid inclusion of false detection in our analyses we only use LPM data if precipitation is simultaneously detected by rain gauges.

The hydrometeor type is detected in 1-minute resolution by the disdrometer. We are especially interested in the type slight and moderate/heavy soft hail (graupel) and hail. Unfortunately, hail is not classified by size, but soft hail is classified by precipitation intensity, I , in three classes; slight soft hail has $I \leq 2,4$ mm/h, moderate soft hail $2,4 < I \leq 12,0$ mm/h, and heavy soft hail has $I > 12,0$ mm/h. The instrument is useful as ground truth for verification of algorithms for radar detection of hail to assess the potential for nowcasting of hail.

INNOVATIONSFONDEN / ØSTERGADE 26 A, 4. SAL / 1100 KØBENHAVN K / W: INNOVATIONSFONDEN.DK
www.rain-erosion.dk

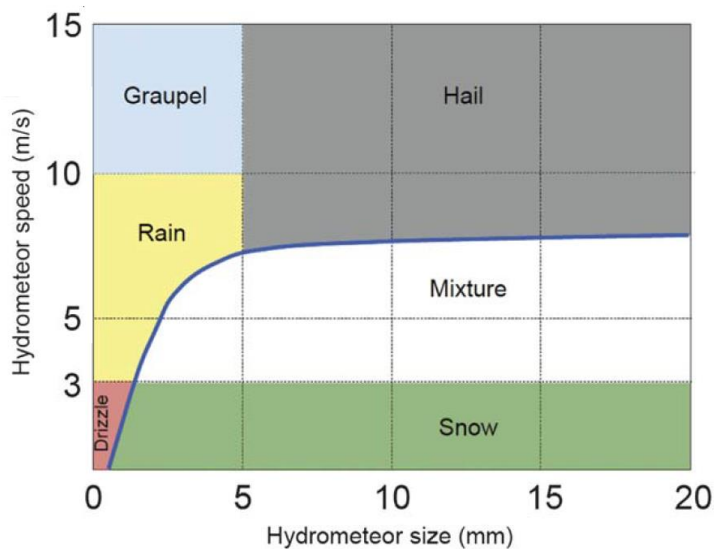


Figure 13. Classification of hydrometeors by particle size versus particle fall speed (Löffler-Mang og Joss, 2000). The thick blue line represents the Gunn-Kinzer line for terminal fall speed for rain drops (Gunn and Kinzer, 1949).

All precipitation events in the period 2012-2018 have been evaluated using rain gauge and disdrometer observations to identify events with occurrence of hail. An event is defined as a hail event if hail is observed in at least one minute, and there have been dry weather at least 20 minutes before and after start and stop of precipitation.

Disdrometer data are complete in most of the period, and there are only breaks in the following seasons: 41,3 % data are missing in autumn 2014, 51,6 % in spring 2015, 1,7 % in winter 2017/18, data are completely missing in spring 2018, and 44,0 % data missing in summer 2018. The average number of minutes with hail and graupel in winter, spring, summer, and autumn for the 7 years period is calculated and we get that the duration of hail and graupel is 3:17 hours per year (Table 2). Hail/graupel is most frequent in spring and summer but is rarely observed in winter. Slight and moderate graupel is observed 0:27 and 2:15 hours, respectively, and hail is observed 35 minutes per year. While slight graupel is practically only observed in spring (20 minutes), moderate graupel are seen more often in spring, summer, and autumn. The statistics on the frequency of ice hydrometeors is interesting in the context of blade erosion since hail/graupel of even short duration can cause large damage. The observed frequency tells us that development of an algorithm for prediction of hail should be given high priority.

Table 2. Number of hours and minutes with hail and graupel (hh:mm) in the period 2012-2018 in Voulund. Winter: December - March. Spring: Marts - May. Summer: June - August. Autumn: September - November.

Hydrometeor type	Winter	Spring	Summer	Autumn	Total
Hail	0:04	0:11	0:15	0:05	0:35
Slight graupel	0:05	0:20	0:01	0:01	0:27
Moderate graupel	0:04	0:34	0:53	0:44	2:15
I ALT	0:13	1:05	1:09	0:50	3:17

Sagsnr. 6154-00018B

Table 3. Statistics on events and days with hail in Voulund in the period 2012-2018. Event statistics: total number of hail events, and average number of events per year. Days: total number of days, and average number of days per year with hail.

Number of		Winter	Spring	Summer	Autumn	Total
Events	Total	16	34	74	56	180
	Year	2,0	4,3	9,3	7,0	22,5
Days	Total	10	25	50	41	126
	Year	1,3	3,1	6,3	5,1	16,0

Table 3 shows the number of days and events with hail in Voulund in the period 2012-2018, given as total number over the whole period and yearly average. The statistics tells us how often we must expect to activate an ESM control in Voulund, i.e., central parts of Jutland, because of hail: 22,5 times/year spread over 16 days. In total, we have identified 180 hail events. In next section, DMI's hail detection algorithm's ability to detect hail will be evaluated for as many as these events as possible.

2.4.2 Evaluation of radar classification of hail for Voulund area

DMI's Probability Of Hail (POH) product is evaluated for the events in as much of the period 2012-2018 as possible. The original probability data have not been stored, but graphics showing the POH level in DK in 10-minute resolution is available most of the time from 2014 onwards. The evaluation is done by manual inspection of the POH level for the area around Voulund which was calculated using data from DMI's Rømø and Virring radars, for which the distance to Voulund is reasonable. POH graphics are missing for some events, but it is possible to evaluate 135 of the 180 events in the period 2012-2018 using Rømø data and 131 events using Virring data. Figure 14 shows an example of POH graphics for 28 July 2018 for the Virring radar. It clearly appears to be difficult to assess an exact POH value from the color level, and therefore, to make it easier, 4 POH classes have been defined (Table 4).

Table 4. POH (Probability Of Hail) classes.

POH class	Probability interval	Probability of hail
1	0-20	Probably none
2	20-40	Low
3	40-60	Intermediate
4	60-100	High

Hail is a local phenomenon associated with convective processes. For example, it has been a challenge in DMI's level 2 hydrometeor classification algorithm to identify hail cells as they may occupy only few pixels and may be contaminated by other hydrometeor classes (Gill et al, 2012a). In other words, we may expect that the POH algorithm may fail detection of hail if the event is characterized by short duration or low amount of precipitation, P_{event} . That is what is seen in the result of the manual evaluation in Table 5.

The percentage of hail events with low P_{event} (< 1 mm) is largest for POH class 1 which is especially evident for the Rømø radar, and for POH class 4 no hail events have less than 1 mm precipitation. The overall average of P_{event} shows a tendency to increase with the POH class which may not be a surprise, but the standard deviation of P_{event} indicates large variations in P_{event} for all classes.

Sagsnr. 6154-00018B

We may also expect that hail causes a clearer signal in the statistics than graupel due to the generally much larger particle size of hail compared to graupel. While the average duration of graupel (-GS and GS in Table 3) shows no clear relation to the POH class, we see a markedly increased duration of hail from 0,3-0,5 minutes/event for POH class 1 to 4,5-6,8 minutes/event for class 4. When the duration of hail is compared to the total duration of the event hail makes up 9-10 % of the total duration for POH class 4 but only 0,2-0,5 % for class 1. The statistics also shows the percentage of events that have no hail (GR) or have 1 or 5 minutes or more with hail. There is a clear tendency that with increasing POH class, there are gradually more events with longer duration of hail. We see that 80-100 % of the events in POH class 4 have ≥ 1 minute with hail and 40-75 % with ≥ 5 minutes with hail. For POH class 1 the corresponding values are 18-25 % and about 1,6 %, respectively.

We notice that despite the simplicity of the manual evaluation method, POH seems to be a pretty good indicator of the risk of hail, which could be used in a hail warning system. It must be noted, that POH should be evaluated more thoroughly on calculated values. In addition, the evaluation has only been carried out for events where the disdrometer observed hail and/or graupel. Since we have no information about the number of misses where hail indicated by radar is not observed at the ground, it does not make sense to calculate probability statistics from a contingency table.

Other useful products in a hail warning system are the Vertical Integrated Ice (VII) and Level 2 Classification products. Graphics for VII is only available for a small number of the hail events and an evaluation was not possible, but for Level 2 Classification graphics are available for the Verring radar for 108 of the hail events in the period 2012-2018. The evaluation was conducted for two classes as a yes/no strategy: hail was not detected (class 1), and hail was detected (class 2).

Table 5. Result of POH evaluation for Verring and Rømø radar data for the period 2014-2018. Rain gauge observations: $p < 1$ (%) = percentage events with precipitation amount < 1 mm, avg, stdev = average and standard deviation of precipitation amount of all events in a class. Hail duration: 0 = pct. events with no hail observed, ≥ 1 = pct. events with hail duration ≥ 1 minute, ≥ 5 pct. events with hail duration ≥ 5 minute, avg = average duration (minutes). Average duration: GR, -GS, GS = average duration (minutes) of hail, slight and moderate graupel. N = number of events.

Radar	POH class	Rain gauge observations			Disdrometer hail duration				Average duration			N
		$p < 1$ (%)	Avg	Stdev	0	≥ 1	≥ 5	Avg	GR	-GS	GS	
Rømø	1	25,00	3,81	4,27	81,7	18,3	1,7	0,3	0,32	0,90	4,48	60
	2	11,11	4,76	4,34	61,1	38,9	5,6	0,9	0,83	0,11	7,33	18
	3	6,38	9,12	12,08	36,2	63,8	8,5	1,3	1,45	0,19	3,21	47
	4	0,00	7,74	8,71	20,0	80,0	40,0	8,6	4,50	0,70	5,50	10
Verring	1	11,29	4,51	4,51	74,2	25,8	1,6	0,5	0,48	0,56	4,10	62
	2	10,34	9,50	16,08	58,6	41,4	6,9	0,7	0,86	0,03	4,97	29
	3	11,11	7,05	7,59	41,7	58,3	5,6	1,9	1,47	0,22	3,22	36
	4	0,00	12,02	10,84	0,0	100,0	75,0	9,7	6,75	0,00	6,75	4

Sagsnr. 6154-00018B

It is seen in Table 6 that when hail is detected by Level 2 Classification most of the statistical measures in the table indicates higher frequency of hail and graupel. There is a marked difference between class 1 and 2. Compared to class 1 there are significantly fewer percentage of events with $P_{event} < 1$ mm in class 2, the average amount of precipitation and the variability is larger, the percentage of events with no disdrometer detection of hail (GS) is smaller, and there are more events with a hail duration ≥ 1 minute. This is particularly evident for hail durations ≥ 5 minutes since 15,2 % of the events in class 2 fall in this group, but that is only the case for 1,6 % in class 1. The average duration of hail (GR) and moderate graupel (GS) in class 2 is larger than in class 1, and for moderate graupel a pronounced difference is seen. The opposite is seen for slight graupel (-GS), which is possibly because the smaller particle size for slight graupel is more difficult to identify by the level 2 classification algorithm compared to moderate graupel and hail.

Table 6. Level 2 Classification of hail for Voulund area based on Virring radar data for the period 2012-2018. Rain gauge observations: $p < 1\%$ = percentage events with precipitation amount < 1 mm, avg = average P_{event} , stdev = standard deviation of P_{event} . Hail duration: 0 = no hail observed (but graupel), ≥ 1 = % events with hail duration ≥ 1 minute, ≥ 5 = % events with hail duration ≥ 5 minutes. Average duration: GR = duration of hail, -GS = duration of slight graupel, GS = duration of moderate graupel. N = number of events.

Level 2 class	Rain gauge observations			Disdrometer hail duration			Average duration			N	
	p<1 %	Avg	Stdev	0	≥ 1	≥ 5	Avg	GR	-GS		GS
1	16,13	4,30	4,84	71,0	29,0	1,6	0,41	0,44	1,21	3,44	62
2	6,52	8,78	14,05	47,8	52,2	15,2	2,19	1,80	0,02	26,00	46

Finally, an example where all hail detection algorithms are in operation (Level 2 Classification, Probability Of Hail, Vertical Integrated Ice) is displayed for an event with observation of severe hail in Voulund on 28 July 2018 (Figure 14). A band of heavy showers passing Voulund from the south had reflectivity as high as 40-45 dBZ in many of the convective cells, locally as high as near 50 dBZ which is very unusual (or unrealistic) for common drop sizes. It may not be a surprise that the Level 2 Classification has detected hail in many places along the shower line. Furthermore, VII shows many cells with large amount of ice in a vertical column of air in the same areas where hail is classified, and in these areas, we also observe POH values $> 70\%$, or locally up to about 90 %.

Sagsnr. 6154-00018B

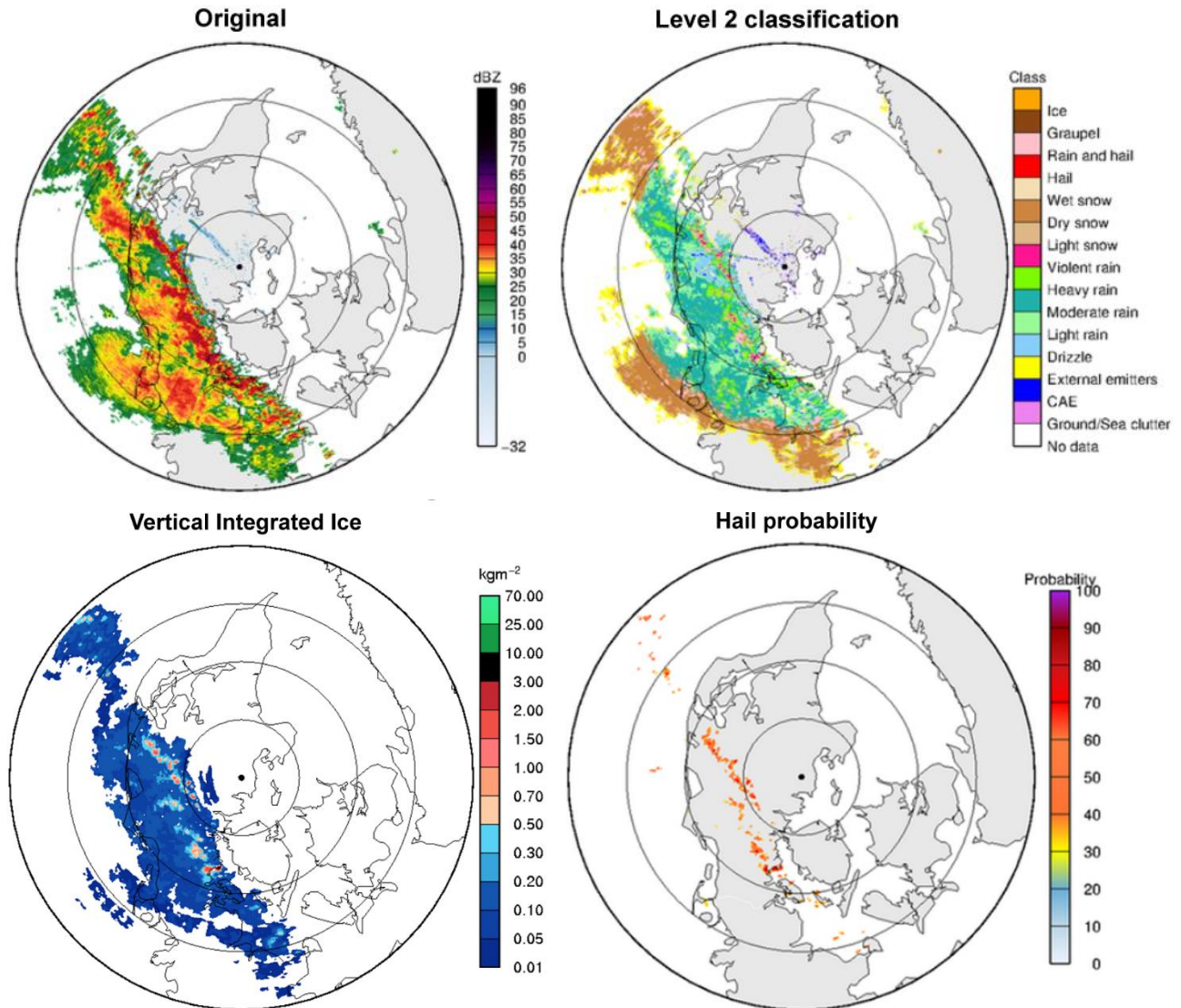


Figure 14. Radar products 28 July 2018 for Verring. Upper left: radar reflectivity. Upper right: classification of hydrometeors and non-meteorological targets. Lower left: vertical integrated ice (kg/m^2). Lower right: probability of hail, POH.

3. Closing remarks

Dual-pol radar products, required or potentially useful for an erosion safe mode (ESM) warning system, are reflectivity (rain rate), hydrometeor classification, vertical integrated ice, and probability of hail. Long time series of rain gauge and disdrometer data in a test field in Voulund have been used for evaluation of nowcasting of radar rain rate and hail detection by radar and have showed promising results.

The results lead us to the conclusion that combination of these radar products could be very useful in a hail warning system, which will thus have a great potential to prevent or reduce damage to wind turbine blades, especially those caused by ice particles like hail.

Due to the lack of agreement between elevated dual-pol radar measurements at larger ranges and the conditions near the ground surface, uncertainties of estimated parameters must be considered and addressed. The challenge is to establish reliable estimates of radar rain rates and hydrometeor classification at the same height as wind farms.

To achieve a reliable nowcasting system for prediction of potentially damaging precipitation types, we may consider the following future improvements: (1) adjustment of radar data by rain gauges to increase reliability of rain rate, (2) develop prediction of hail by combination of relevant radar products, (3) inclusion of other at the moment experimental radar products like fall velocity and particle size, (3) spatial graduation of alarm level within nowcasting area and activation of alarms in sub-sections of a wind farm as illustrated below, (4) make the warning system more robust to spatial variability of weather and precipitation type.

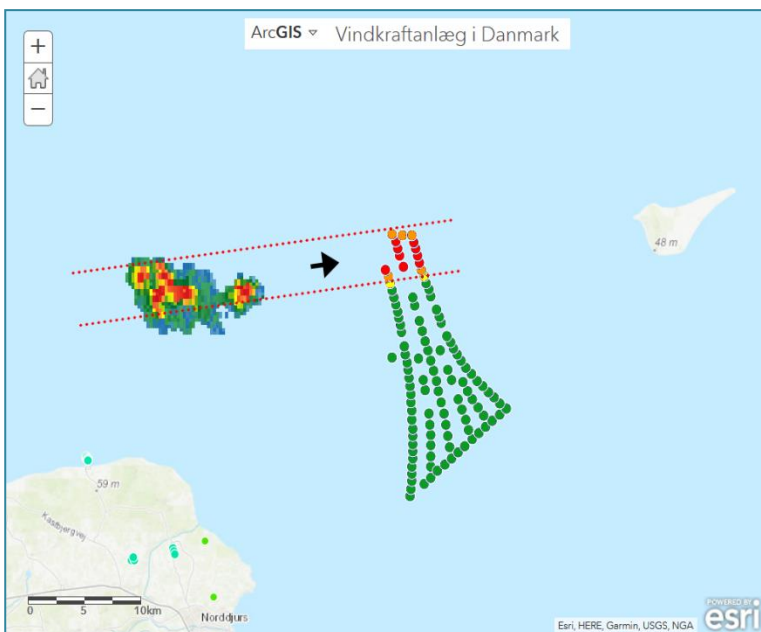


Figure 15. Spatial graduation of alarm level in sub-sections of a wind farm. Green = no alarm. Yellow, orange, red = increasing level of expected severity of rain rate.

References

- Assouline, S.: Dop size distributions and kinetic energy rates in variable intensity rainfall. *Water Res. Research*, Vol. 45, W11501, doi:10.1029/2009WR007927, 2009.
- Battan, L. J.: Radarobservation of the atmosphere. *The University of Chicago Press, Chicago*, p. 1-113, 1972.
- Best, A. C.: The size of distribution of raindrops, *Quart. J. R. Met. Soc.*, 76, p. 16, 1950.
- Bowler, N. E., Pierce, C. E. and Seed, A. W.: STEPS: A probabilistic precipitation forecasting scheme. *Quarterly Journal of the Royal Meteorological Society*, 132: 2127-2155, 2006.
- Bradski, G. and Kaehler, A.: *Learning OpenCV. O'Reilly Media, 2008.*
- Brandes, E. A.: Optimizing rainfall estimates with the aid of radar. *J. Appl. Meteorol.*, 14, 1339–1345, 1975.
- Chumchean, S., Sharma, A., Seed, A.: An integrated approach to error correction for real-time radar-rainfall estimation. *J. Atmos. Ocean. Technol.* 23:67–79, 2006.
- De Haijn, M. and Wauben, W.: Investigation into improvement of automated precipitation type of observation at KNMI. In: TECO 2010- WMO Technical Conference on Meteorological and Environmental Instruments and Methods of Observation, Helsinki, Finland 30.8.-1.9.2010. World Meteorological Organisation, Instruments and observing methods, IOM No. 104. 3(2), 2010.
- Delobbe, L., Bastin, G., Dierickx, D., Goudenhoofdt, E., Leclercq, G., Moens, L., and Thunus, M.: Evaluation of several radar-gauge merging techniques for operational use in the Walloon region of Belgium. https://www.researchgate.net/publication/228466330_Evaluation_of_several_radar-gauge_merging_techniques_for_operational_use_in_the_Walloon_region_of_Belgium/download, 2008.
- Ebert, E. E.: Fuzzy verification of high-resolution gridded forecasts: a review and proposed framework. *Met. Appl.*, 15: 51-64, 2008.
- Gabella, M., and Amitai, E.: Radar rainfall estimates in an alpine environment using different gage-adjustment techniques. *Phys. Chem. Earth B*. 25:927–931, 2000.
- Gill, R. S., 2010: DMI Radar Operational Products System (DROPS). DROPS - release 1.0. DMI Intern Rapport 10-6, København 2010, 23pp.
- Gill, R. S., Overgaard, S., and Bøvith, T., 2008: "Evaluation of the dual polarisation radar in an operational network", ERAD 2008, 5th European conference on Radar in Meteorology and Hydrology, oral presentation.
- Gill R. S., Bøvith, T., Sørensen, M. B., Overgaard, S., and Michelson, D., 2010: "Development and evaluation of a BALTRAD dual polarisation hydrometeor classifier", ERAD 2010, 6th European conference on Radar in Meteorology and Hydrology, oral presentation.
- Gill, R., Sørensen, M. B., Bøvith, T., 2012a: Hydrometeor Classification using Polarimetric C-band Doppler Weather Radars. *DMI Scientific Report 12-04*, 29 p., 2012.

Sagsnr. 6154-00018B

Gill, R. S., Sørensen, M. B., Bøvith, T., Koistinen, J., Peura, M., Michelson, D., and Cremonini, R., 2012b: "BALTRAD dual polarization hydrometeor classifier", ERAD 2012, 7th European conference on Radar in Meteorology and Hydrology.

Goudenhoofdt, E, and L. Delobbe: Evaluation of radar-gauge merging methods for quantitative precipitation estimates. *Hydrol. Earth Syst. Sci.*, 13, 195–203, 2009.

Gunn, R., and G. Kinzer: The terminal velocity of fall for water droplets in stagnant air. *J. Meteor.*, **6**, 243-248, 1949.

Haberlandt, U.: Geostatistical interpolation of hourly precipitation from rain gauges and radar for a large-scale extreme rainfall event. *J. Hydrol.* 332:144–157, 2007.

Hasager, C., and Vejen, F.: Disdrometers in EROSION. Deliverable D1.1 (Public), Innovationsfonden, Sagsnr. 6154-0018B, 2017, 9 pp.

Hasager, C., F. Vejen, J. I. Bech, W. R. Zkrzypínski, A.-M. Tilg, M. Nielsen: Assessment of the rain and wind climate with focus on wind turbine blade leading edge erosion rate and expected lifetime in Danish Seas. *Renewable Energy*, Vol. 149, April 2020, 91-102.

Holleman, I.: Hail detection using single-polarization radar, Scientific Report, KNMI WR-2001-01, 2001, 72pp.

Delobbe, L. & Holleman, I.: Radar-based hail detection: Impact of height assignment errors on the measured vertical profiles of reflectivity. In Preprints 31st Conference on Radar Meteorology, Seattle, WA, Am. Meteorol. Soc. 475–478, 2003.

Karlsson, K.-G.: An Introduction to Remote Sensing in Meteorology. SMHI, 1997, 315pp.

Kubilay, A., Derome, D., Blocken, B., Carmeliet, J.: CFD simulation and validation of wind-driven rain on a building facade with an Eulerian multiphase model. *Build. Environ.*, vol. 61, 69–81, <http://dx.doi.org/10.1016/j.buildenv.2012.12.005>, 2013.

Löffler-Mang, M., and J. Joss: An optical disdrometer for measuring size and velocity of hydrometeors. *J. Atmos. Technol.*, 2000, 17(2), 130-139.

Maddox, R.A., D.S. Zaras, P.L. MacKeen, J.J. Gourley, R. Rabin, and K.W. Howard: Echo height measurements with the WRS-88D: Use of data from one versus two radars. *Wea. Forecasting*, **14**, 455-460, 1999.

Marshall, J. S., and W. McK. Palmer: The distribution of raindrops with size. *J. Meteor.*, vol. 5, 165-166, 1948.

Marshall, J.S., Hitschfeld, W. and Gunn, K.L.S.: Advances in radar weather. *Adv. Geophys.*, 2, 1–56, 1955.

Michelson, D. B., T. Andersson, J. Koistinen, C. G. Collier, J. Riedl, J. Szturc, U. Gjertsen, A. Nielsen, S. Overgaard: BALTEX Radar Data Centre Products and their Methodologies. *SMHI Reports Meteorology and Climatology*, RMK No. 90, 75p, 2000.

Sagsnr. 6154-00018B

Michelson D., Szturc J., Gill R.S., Peura M: “Community-based weather radar networking with BALTRAD”, *ERAD 2010, 6th European conference on Radar in Meteorology and Hydrology, 2010*.

Šálek, M., Cheze, J.-L., Handwerker, J., Delobbe, L., Uijlenhoet, R.: Radar techniques for identifying precipitation type and estimating quantity of precipitation. *Document of COST Action 717, WG 1, Task WG 1-2, 51p, 2004*.

Sinclair, S., and G. Pegram: Combining radar and rain gauge rainfall estimates using conditional merging. *Atmos. Sci. Lett. 6:19–22, 2005*.

Straka, J. M., Zrníc, D. S., Ryzhkov, A. V.: Bulk Hydrometeor Classification and Quantification Using Polarimetric Radar Data: Synthesis of Relations. *J. Appl. Met., Vol. 39, 1341-1372, 2000*.

Rosenfeld, D., Wolff, D. B. , Amitai, E.: The window probability matching method for rainfall measurements with radar. *J. Appl. Meteorol. 33:682–693, 1994*.

Uijlenhoet, R.: Raindrop size distributions and radar reflectivity-rain rate relationships for radar hydrology. *Hydrol. Earth Syst. Sci., 5, 615-627, 2001*.

Vejen, F., Bøvith, T., and Gill, R.: Regional precipitation erosion forecast (data). Deliverable D3.2 (Public), Innovationsfonden, Sagsnr. 6154-0018B, 2019, 23 pp.

Vejen, F., Tilg, A.-M., Nielsen, M., & Hasager, C.: Precipitation Statistics for Selected Wind Farms. Deliverable D1.2 (Public), Innovationsfonden, Sagsnr. 6154-0018B, 2018, 37 pp.

Vejen, F., Bøvith, T., and Gill, R.: Regional precipitation erosion forecast (data). Deliverable D3.2 (Public), Innovationsfonden, Sagsnr. 6154-0018B, 2019, 23 pp.

Wauben, W.; Mathijssen, T.; Oudshoorn, C. Field evaluation of sensors for precipitation type discrimination. In Proceedings of the WMO Technical Conference on Meteorological and Environmental Instruments and Methods of Observation (CIMO TECO 2016), Madrid, Spain, 27–30 September 2016, 29pp.